Nano Energy 32 (2017) 1–9

Contents lists available at ScienceDirect

Nano Energy

journal homepage: www.elsevier.com/locate/nanoen

# Freestanding hollow double-shell Se@$CN_x$ nanobelts as large-capacity and high-rate cathodes for Li-Se batteries

Qifa Cai[a], Yuanyuan Li[a], Lei wang[a], Qingwei Li[a,c], Juan Xu[a], Biao Gao[b], Xuming Zhang[b,c], Kaifu Huo[a,*], Paul K. Chu[c]

[a] Wuhan National Laboratory for Optoelectronics and School of Optical and Electronic Information, Huazhong University of Science and Technology, Wuhan 430074, China
[b] The State Key Laboratory of Refractories and Metallurgy, Wuhan University of Science and Technology, Wuhan 430081, China
[c] Department of Physics and Materials Science, City University of Hong Kong, Tat Chee Avenue, Kowloon, Hong Kong, China

ARTICLE INFO

*Keywords:*
Se
Hollow nanobelts
Li-Se battery
Nanocomposites
Freestanding electrode
Electrochemistry

ABSTRACT

Selenium (Se) is a promising cathode material in high-energy batteries. However, the polyselenides shuttle effect and large volume change of Se upon cycling as well as the poor ionic and electronic conductivity of Se undermine its cycling and rate performance. Herein, we report a novel Se-based cathode material in which Se is fully encapsulated and attached to the inner shell of hollow-core nitrogen-doped carbon ($CN_x$) nanobelts forming hollow double-shell Se@$CN_x$ nanobelts with a well-defined inner-void volume. Such novel electrode material could accommodate the large volume variation of Se upon cycling and facilitate electron and ion transfer while providing a physical entrapment for the Se and polyselenide intermediates, thereby producing large capacity, high rate capability and long-lifespan. With a large Se content of 62.5 wt% and areal mass loading of 3.0 mg $cm^{-2}$, the freestanding and binder-free Se@$CN_x$ cathode comprising of intertwining and interpenetrating hollow double-shell Se@$CN_x$ nanobelts could deliver a high capacity of 608.8 mAh $g^{-1}$ at a density of 675 mA $g^{-1}$ and the cycle stability is maintained for over 400 cycles with only 0.06% capacity decay per cycle. When the current density is increased 20 times from 80 to 1600 mA $g^{-1}$, 70% reversible capacity is retained.

## 1. Introduction

The ever-increasing market demand for mobile electronics, electric vehicles (EVs), and large-scale renewable energy storage has spurred rapid development of rechargeable lithium-ion batteries (LIBs) [1–9]. However, the current LIBs suffer from small energy densities due to the low specific capacity of the graphite anode and $LiCoO_2$/$LiFeO_4$ cathodes and may not suffice for future electric vehicles (EVs) and grid energy storage [10–12]. The Li-S battery has a large theoretical energy density of 2600 Wh $kg^{-1}$ which is much bigger than those of commercially available LIBs such as $LiCoO_2$/graphite and $LiFePO_4$/graphite [13]. Additionally, S is quite abundant, cheap, and environmentally friendly [14]. Hence, Li-S batteries have aroused much interest as next-generation high-energy rechargeable batteries. However, the commercialization of Li-S batteries batteries is hindered by some practical drawbacks such as the low conductivity of S and its discharge products, high solubility of the polysulfide intermediates ($Li_2S_n$, n > 2) in the electrolyte, thus resulting in rapid capacity decay and undermining rate performance [15–18].

Selenium (Se) has a multi-electron electrochemical redox reaction mechanism similar to that of S but has higher conductivity. The conductivity of Se ($1\times10^{-3}$ S $m^{-1}$) is larger than that of S ($5\times10^{-28}$ S $m^{-1}$ at 25 °C) giving rise to better electrochemical properties in batteries including higher utilization rate and faster electrochemical reaction rate [19]. On the other hand, although the theoretical gravimetric capacity of Se (675 mAh $g^{-1}$) is smaller than that of S (1672 mAh $g^{-1}$), Se has a high volumetric capacity (3253 Ah $L^{-1}$ based on 4.82 g $cm^{-3}$) comparable to S (3467 Ah $L^{-1}$ based on the density of 2.07 g $cm^{-3}$) due to the large density of Se [20]. Moreover, Se is more compatible with cost-effective carbonate-based electrolytes whereas S is largely limited to expensive ether-based electrolytes [19]. Despite the perceived advantages of Li-Se batteries, dissolution and shuttle effect of intermediates in Li-S batteries also plague Li-Se batteries [21]. On the other hand, the large volumetric change (about 150% assuming full lithiation from Se to $Li_2Se$) of Se during charging and discharging causes pulverization, structural damage, loss of Se active materials and capacity degradation [22].

To overcome these hurdles, hollow carbon spheres, carbon nano-

* Corresponding author.
*E-mail address:* kfhuo@hust.edu.cn (K. Huo).

http://dx.doi.org/10.1016/j.nanoen.2016.12.010
Received 6 October 2016; Received in revised form 23 November 2016; Accepted 6 December 2016
Available online 07 December 2016

**Table 1**
Performance comparison of hollow double-shell Se@$CN_x$ nanobelts with other Se/C composites for application in Li-Se Batteries.

| Material | Se content in the composite | Se content in the cathode | Areal Se mass loading | [Capacity and cycle][a] | Ref. |
|---|---|---|---|---|---|
| Se/CMK-3 | 49 wt% | 39.2 wt% | 2 mg $cm^{-2}$ | 600 mAh $g^{-1}$ after 50 cycles at 0.1 C | [23] |
| Se/mesoporous carbon | 30 wt% | 24 wt% | ____ | 480 mAh $g^{-1}$ after 1000 cycles at 1 C | [20] |
| Graphene-Se/CNT | 30 wt% | 30 wt% | ____ | 315 mAh $g^{-1}$ after 100 cycles at 0.1 C | [38] |
| Se/carbon aerogel | 56.0 wt% | 44.8 wt% | 1.5–2.0 mg $cm^{-2}$ | 309 mAh $g^{-1}$ after 100 cycles at 0.5 C | [39] |
| Se/porous carbon sphere | 70.5 wt% | 56.4 wt% | 2 mg $cm^{-2}$ | 417 mAh $g^{-1}$ after 1200 cycles at 1 C | [24] |
| Se/mesoporous carbon sphere | 50 wt% | 40 wt% | ____ | 300 mAh $g^{-1}$ after 100 cycles at 0.5 C | [40] |
| Se/nitrogen-doped microporous carbon spheres | 50.0 wt% | 35.0 wt% | 2 mg $cm^{-2}$ | 570 mAh $g^{-1}$ after 350 cycles at 0.5 C | [41] |
| Se/hollow porous carbon spheres | 48.68 wt% | 38.9 wt% | ____ | 200 mAh $g^{-1}$ after 1000 cycles at 1 C | [42] |
| core-shell structured selenium@ carbon spheres | 68 wt% | 54.4 wt% | 1–2 mg $cm^{-2}$ | 300 mAh $g^{-1}$ after 100 cycles at 0.1 C | [37] |
| Hollow double-shell Se@$CN_x$ nanobelts | 62.5 wt% | 62.5 wt% | 3.0 mg $cm^{-2}$ | 453.2 mAh $g^{-1}$ after 400 cycles at 800 mA $g^{-1}$ | This work |

[a] Capacity based on the mass of Se (1 C=675 mA $g^{-1}$).

fibers, mesoporous carbon, or graphene have been proposed as host materials for Se in order to improve the cathodic properties of Se. For example, Guo et al. confined Se in an ordered mesoporous carbon (CMK-3) matrix to obtain a large capacity of 600 mAh $g^{-1}$ at a current density of 67 mA $g^{-1}$ [23]. Huang et al. prepared Se-loaded N-doped microporous carbon and the composite delivered a capacity of 462 mA h $g^{-1}$ at 1 C (675 mA $g^{-1}$) after 150 cycles [24]. Currently, Se/C composites are mainly prepared by the melt-diffusion method after the carbon structures have been prepared and they generally have a relatively low Se content (generally ≤50%) in the cathode (See Table 1) resulting in low overall capacity and energy density based on the whole cathode. On the other hand, most of Se is not fully encapsulated into the C host but generally coated on the surface in the reported Se/C composite. Since the Se in the Se/C composites could still be accessed by electrolyte in which polyselenides could be dissolved, the Se active material loss and polyselenides shuttle phenomenon could only be alleviated, but not eliminated. Moreover, compared to S, Se suffers from larger volume variation during the cycle process, which causes fracture and pulverization of the Se active materials and even destruction of the cathode structure. Furthermore, most Se/C composites require conductive additives, polymetric binders, and metallic current collectors to prepare the cathodes but they decrease the proportion of Se in the cathode and consequently the energy density of the Li-Se batteries. The ideal scenario for the Se cathode material is to design a C coated Se (Se@C) nanostructure that has a controlled void volume to buffer the large volumetric change of Se during charging/discharging and effectively traps the Se and $Li_2Se_x$ species in the cathode while at the same time has a large Se content and high utilization even at high current densities. Unfortunately, such perspective Se@C cathode material has not been reported to date.

Herein, we report the rational design and fabrication of a novel Li-Se cathode material in which Se is fully encapsulated and attached to the inner shell of hollow-core nitrogen-doped carbon ($CN_x$) nanobelts forming hollow double-shell Se@$CN_x$ nanobelts with a well-defined inner-void volume as schematically shown in Scheme 1. The hollow double-shell Se@$CN_x$ nanobelts are prepared by oxidizing the as-synthesized core-shell ZnSe@$CN_x$ nanobelts by $FeCl_3$ and ZnSe is transformed into elemental Se and $Zn^{2+}$ by the reaction of ZnSe(s) +2$Fe^{3+}$(aq.)=$Zn^{2+}$(aq.)+ Se(s) +2$Fe^{2+}$(aq.). The *in situ* formed Se are fully encapsulated and attached to the inner shell of $CN_x$ shells with free $Zn^{2+}$ and $Fe^{2+}$ leached into the solution through the micropores on the $CN_x$ shells. The 1D hollow double-shell Se@$CN_x$ composite has several advantages. First of all, in contrast to the conventional melt-diffusion method, our technique can fully encapsulate Se inside the highly conductive $CN_x$ shell with a controlled void volume which can accommodate the large volume expansion of Se and effectively trap the Se and polyselenides intermediates during charging/discharging. Secondly, the 1D double-shell Se@$CN_x$ nanobelts increase the electroactive interface to facilitate transfer of ions and electrons and increase the utilization of Se, thereby producing high capacity and rate capability. Thirdly, with an ultrahigh aspect ratio, the double-shell Se@$CN_x$ nanobelts can readily form a self-supporting film with a 3D interconnected conductive network by the simple vacuum-filtration method without the need of a binder or conducting additives. The binder-free freestanding Se@$CN_x$ electrode film comprising intertwining and interpenetrating hollow double-shell Se@$CN_x$ nanobelts is adopted as the cathode in a Li-Se battery, which increases the Se content in the cathode and the 3D structure facilitates electron and ion transfer during charging/discharging. With a large Se content of 62.5 wt% and areal mass loading of 3.0 mg $cm^{-2}$, the freestanding Se@$CN_x$ cathode delivers a high capacity of 608.8 mAh $g^{-1}$ at a density of 675 mA $g^{-1}$ and maintains a long cycling stability and an excellent rate capability, rendering promising applications in Li-Se batteries.

## 2. Experimental section

### 2.1. Preparation of hollow double-shell Se@$CN_x$ nanobelts

#### 2.1.1. Synthesis of core-shell ZnSe@$CN_x$ nanobelts

The ZnSe[DETA]$_{0.5}$ nanobelts were prepared by a modified hydrothermal method [25]. In the typical synthesis, 0.5 mmol of $ZnSO_4 \cdot 7H_2O$ and 0.5 mmol of $Na_2SeO_3$ were added to an aqueous solution containing diethylenetriamine (DETA) and hydrazine hydrate ($N_2H_4 \cdot H_2O$) with a volume ratio of $V_{N2H4 \cdot H2O}/V_{DETA}/V_{H2O}$=5:14:16 under magnetic stirring. The solution was sealed in a 40 mL Teflon-lined autoclave and maintained in an oven at 180 °C for 24 h. After cooling to room temperature naturally, the white floccules were obtained by filtration and washed with distilled water (DW) and absolute alcohol several times. Finally, the ZnSe[DETA]$_{0.5}$ nanobelts were dried at 80 °C for 6 h under vacuum.

To prepare the core-shell ZnSe@$CN_x$ nanobelts, 200 mg of the ZnSe[DETA]$_{0.5}$ nanobelts were dispersed in DW at a concentration of 0.5 mg $mL^{-1}$. After stirring for half an hour, 484 mg of Tris(Tris(hydroxymethyl)aminomethane) were added to the solution under stirring and then 400 mg of 3-hydroxytyramine hydrochloride were added to the solution. After 1 h reaction, polydopamine (PDA) coated ZnSe[DETA]$_{0.5}$ nanobelts were produced. The as-synthesized ZnSe[DETA]$_{0.5}$@PDA nanobelts were further carbonized at 700 °C for 2 h under Ar to produce core-shell ZnSe@$CN_x$ nanobelts.

#### 2.1.2. Synthesis of hollow double-shell Se@$CN_x$ nanobelts

The as-prepared ZnSe@$CN_x$ nanobelts were immersed into aqueous solution of $FeCl_3$ for over 10 h under stirring at room temperature to produce hollow double-shell Se@$CN_x$ nanobelts. The inner core of

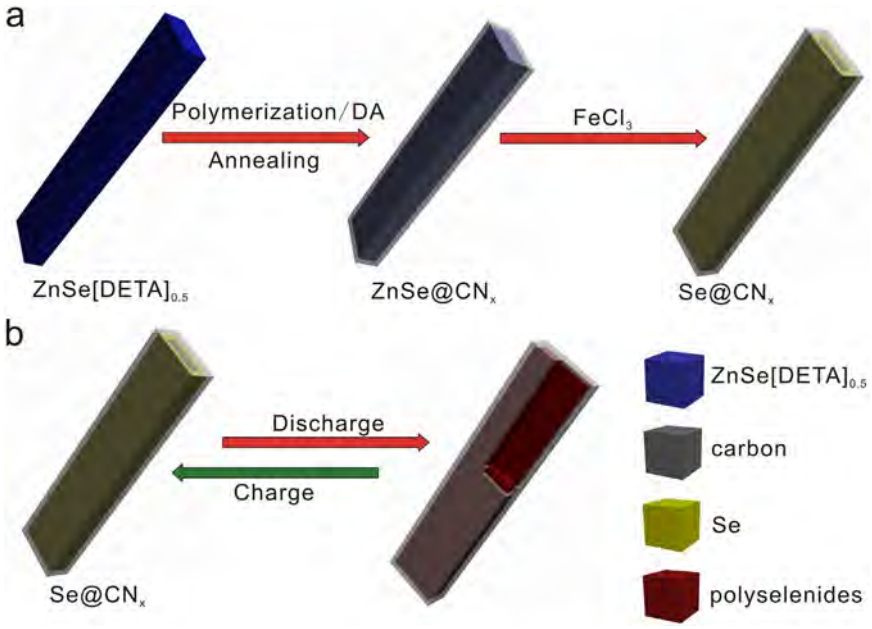


**Scheme 1.** (a) Preparation procedures of the hollow double-shell Se@$CN_x$ nanobelts and (b) advantages of the hollow double-shell Se@$CN_x$ nanobelts for Li-Se batteries.

ZnSe is oxidized to Se by the reaction of ZnSe(s) +2$Fe^{3+}$(aq.) =$Zn^{2+}$(aq.)+Se(s)+2$Fe^{2+}$(aq.) with free $Zn^{2+}$ and $Fe^{2+}$ leached out into the solution through the micropores of the carbon shells during subsequent washing. The freestanding Se@$CN_x$ cathode film comprising of intertwining and interpenetrating hollow double-shell Se@$CN_x$ nanobelts was prepared *via* vacuum filtration without needing a foreign binder or conducting additives.

### 2.2. Structural and morphology characterization

The morphology, structure, and composition of the ZnSe[DETA]$_{0.5}$, core-shell ZnSe@$CN_x$ and hollow double-shell Se@$CN_x$ composites were characterized by X-ray diffraction (XRD, Bruker AXS D2 Phaser) with Cu $K_\alpha$ radiation, field-emission scanning electron microscopy (FE-SEM, FEI NanoSEM 450), transmission electron microscopy (TEM, FEI Titan 60–300 Cs), high-resolution TEM (HR-TEM, Titan), Raman scattering (HR RamLab) and X-ray photoelectron spectroscopy (XPS, ESCALB MK-II, VG Instruments, UK) using monochromated Mg $K_\alpha$ X-ray. The Se content in the Se@$CN_x$ was determined by thermogravimetric analysis (TGA, NETZSCH; TG 209 F3) in Ar obtained at a heating rate of 10 °C $min^{-1}$. The nitrogen adsorption and desorption isotherms were determined by the Brunauer-Emmett-Teller (BET) (Micrometrics, ASAP2010) method after degassing the samples at 383 K for 5 h.

### 2.3. Electrochemical tests

The electrochemical properties of the freestanding hollow double-shell Se@$CN_x$ cathodes were evaluated *via* 2025-type coin cells with Li foil as anode. The electrolyte is 1 M $LiPF_6$ in a 1:1 vol/vol mixture of ethylene carbonate (EC) and diethyl carbonate (DEC) and the separator is Celgard 2400 membrane. The charging and discharging profiles were conducted on the MTI automatic battery cyclers with a voltage cut-off between 0.8 and 3.0 V *vs.* $Li/Li^+$. The specific capacity was calculated based on the mass loading of Se in the electrode. The selenium areal loading in the cathode was approximately 3.0 mg $cm^{-2}$. Cyclic voltammetry (CV) was conducted on the CHI 660e electrochemical workstation and the electrochemical impedance spectra (EIS) were acquired on an Autolab electrochemical workstation between 10 mHz and 0.1 MHz.

## 3. Results and discussion

The synthesis procedures of the hollow-core double-shell Se@$CN_x$ nanobelts are illustrated in Scheme 1. Firstly, the diethylenetriamine (DETA)-assisted solvothermal approach was used to synthesize the inorganic-organic hybrid ZnSe[DETA]$_{0.5}$ nanobelts [25]. Figs. 1a-b and S1a (Supporting information) are field-emission scanning electron microscopy (FE-SEM) and transmission electron microscopy (TEM) images of as-synthesized ZnSe[DETA]$_{0.5}$ revealing a nanobelt-like morphology with a rectangular cross-section. The ZnSe[DETA]$_{0.5}$ nanobelts have a width of 200–400 nm and the length and thickness of 10–15 μm and 40–50 nm, respectively. Energy-dispersive X-ray spectroscopy (EDS, Fig. S1b, Supporting information) discloses that the nanobelts consist of Zn, Se, C and N and the X-ray diffraction (XRD) pattern (Fig. S2a, Supporting information) shows an orthorhombic ZnSe[DETA]$_{0.5}$ phase [25], further confirming the formation of ZnSe[DETA]$_{0.5}$ nanobelts. The ZnSe[DETA]$_{0.5}$ nanobelts were subsequently coated with a thin polydopamine (PDA) by dopamine self-polymerization in a Tris buffer (pH=8.5) solution containing dopamine. After thermal calcination under Ar at 700 °C, the PDA coating was carbonized into the $CN_x$ shell to produce the core-shell ZnSe@$CN_x$ nanobelts. The FE-SEM image shown in Fig. 1c reveals that the core-shell ZnSe@$CN_x$ inherits the morphology of the nanobelt-like ZnSe[DETA]$_{0.5}$. However, the inner core of ZnSe becomes coarse due to evaporation and partial carbonization of DETA in the ZnSe[DETA]$_{0.5}$ nanobelts. The corresponding XRD peaks (Fig. S2a, Supporting information) originate from hexagonal ZnSe (JCPDS 15-0105) and the diffraction peaks of ZnSe[DETA]$_{0.5}$ disappear, suggesting that ZnSe[DETA]$_{0.5}$ has been fully transformed into ZnSe. No carbon peaks can be detected by XRD possibly due to the disordered nature of carbon. The core-shell structure of ZnSe@$CN_x$ is further confirmed by the TEM image in Fig. 1d and Raman scattering spectrum (Fig. S2b, Supporting information) and the outer $CN_x$ shell has a uniform thickness of 15–20 nm. The double-shell hollow Se@$CN_x$ nanobelts were obtained by immersing the core-shell ZnSe@$CN_x$ nanobelts in a mild oxidant aqueous solution of $FeCl_3$. The inner core of ZnSe is oxidized to Se by the reaction of ZnSe(s)+2$Fe^{3+}$(aq.) =$Zn^{2+}$(aq.)+Se(s)+2$Fe^{2+}$(aq.) with free $Zn^{2+}$ and $Fe^{2+}$ leached out into the solution through the micropores of the carbon shells leaving voids inside the highly conductive $CN_x$ shells. The FE-SEM (Fig. 1e) and TEM image (Fig. 1f) clearly demonstrate that *in-situ* formed Se

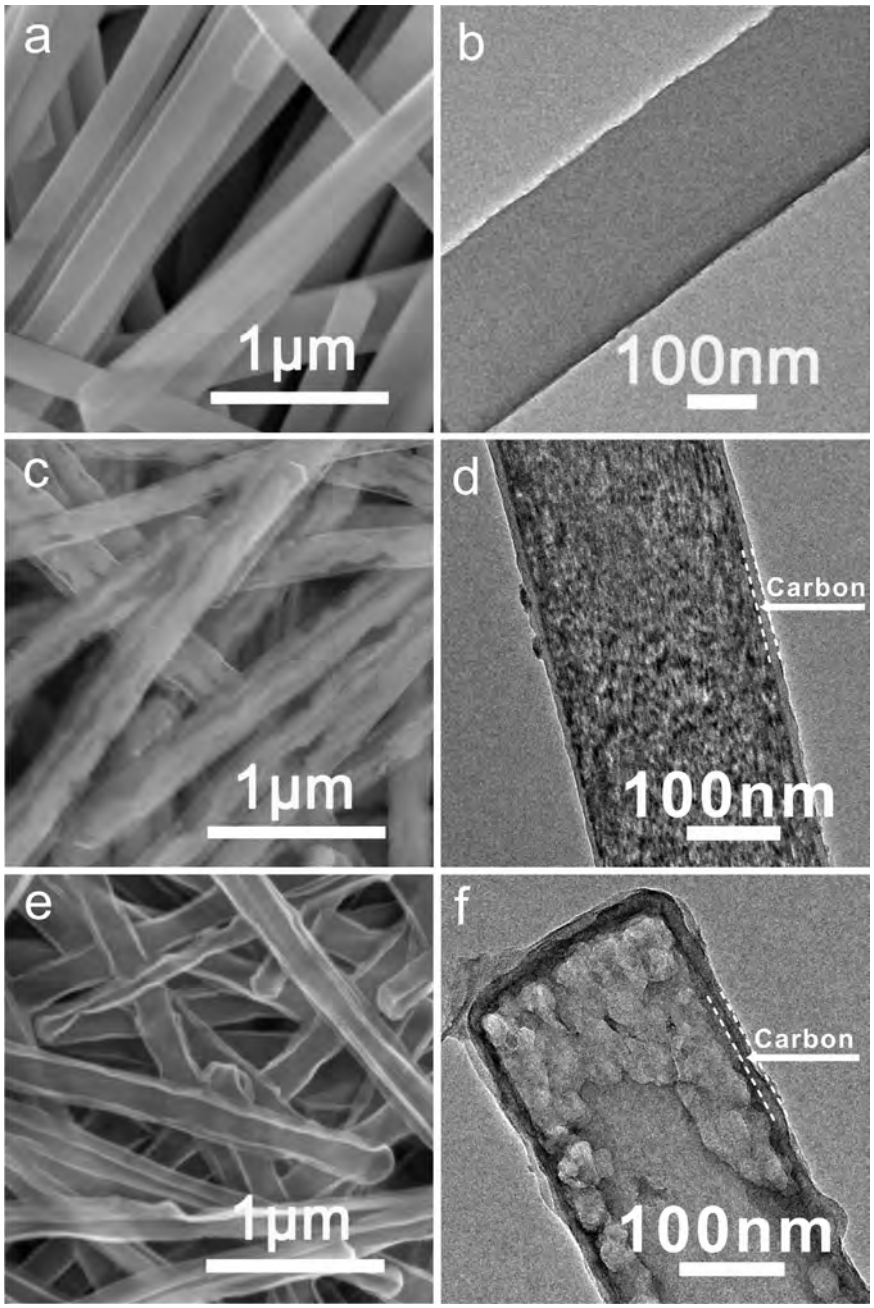


**Fig. 1.** FE-SEM and TEM images of (a, b) $ZnSe[DETA]_{0.5}$ nanobelts, (c, d) core-shell $ZnSe@CN_x$ nanobelts, and (e, f) hollow double-shell $Se@CN_x$ nanobelts.

nanoparticles are fully encapsulated and attached to the inner wall of the hollow $CN_x$ nanobelts leading to the formation of hollow double-shell $Se@CN_x$ nanobelts. FE-SEM image (Fig. S3, Supporting information) indicates that the hollow double-shell $Se@CN_x$ nanobelt has a rectangular cross-section and the thickness and length $Se@CN_x$ are 70–90 nm and 10–15 μm, respectively. EDS (Fig. S4, Supporting information) reveals that the product comprises Se, C and N and no Zn can be detected providing evidence of Zn leaching and removal during the post-purification process. The XRD pattern of $Se@CN_x$ nanobelt show the *in-situ* Se is amorphous (Fig. S2a, Supporting information). The Raman spectrum of the hollow double-shell $Se@CN_x$ (Fig. S2b, Supporting information**)** nanobelts shows a broad peak at 250 $cm^{-1}$ corresponding to disordered chain-like Se molecules [26–29], further indicating that Se is amorphous and the two strong bands at 1350 $cm^{-1}$ and 1585 $cm^{-1}$ are attributed to the $CN_x$ shell [30,31].

The hollow double-shell $Se@CN_x$ nanobelts are further investigated by high-resolution TEM and EDS mapping. Fig. 2a and b disclose the hollow double-shell structures with the thicknesses of C and Se being about 17 and 15 nm, respectively. The EDS line scans and elemental maps (Fig. 2c and d) indicate that C and N are uniformly distributed throughout the nanobelts and Se adheres to the inner wall of the hollow $CN_x$ nanobelts, further confirming the formation of hollow double-shell $Se@CN_x$ nanobelts. The X-ray photoelectron spectroscopy (XPS) and nitrogen adsorption/desorption of double-shell $Se@CN_x$ are also determined. The XPS survey spectrum (Fig. S5a, Supporting information) shows the presence of Se, C, N, and O. The fine XPS of Se is depicted in Fig. 2e and the two strong peaks at 55.9 and 55.0 eV are assigned to Se $3d_{3/2}$ and Se $3d_{5/2}$ of element Se with a spin-orbit splitting of 0.86 eV, respectively [32]. The weak peak at 58.8 eV is attributed to Se-O as a result of surface oxidation [33]. The N1s peaks shown in Fig. 2f can be deconvoluted into three peaks at 398.4, 399.6, and 400.9 eV corresponding to pyridinic, pyrrolic, and quaternary nitrogen, respectively [34]. The XPS results further support the formation of $Se@CN_x$. The surface area and pore distribution of the

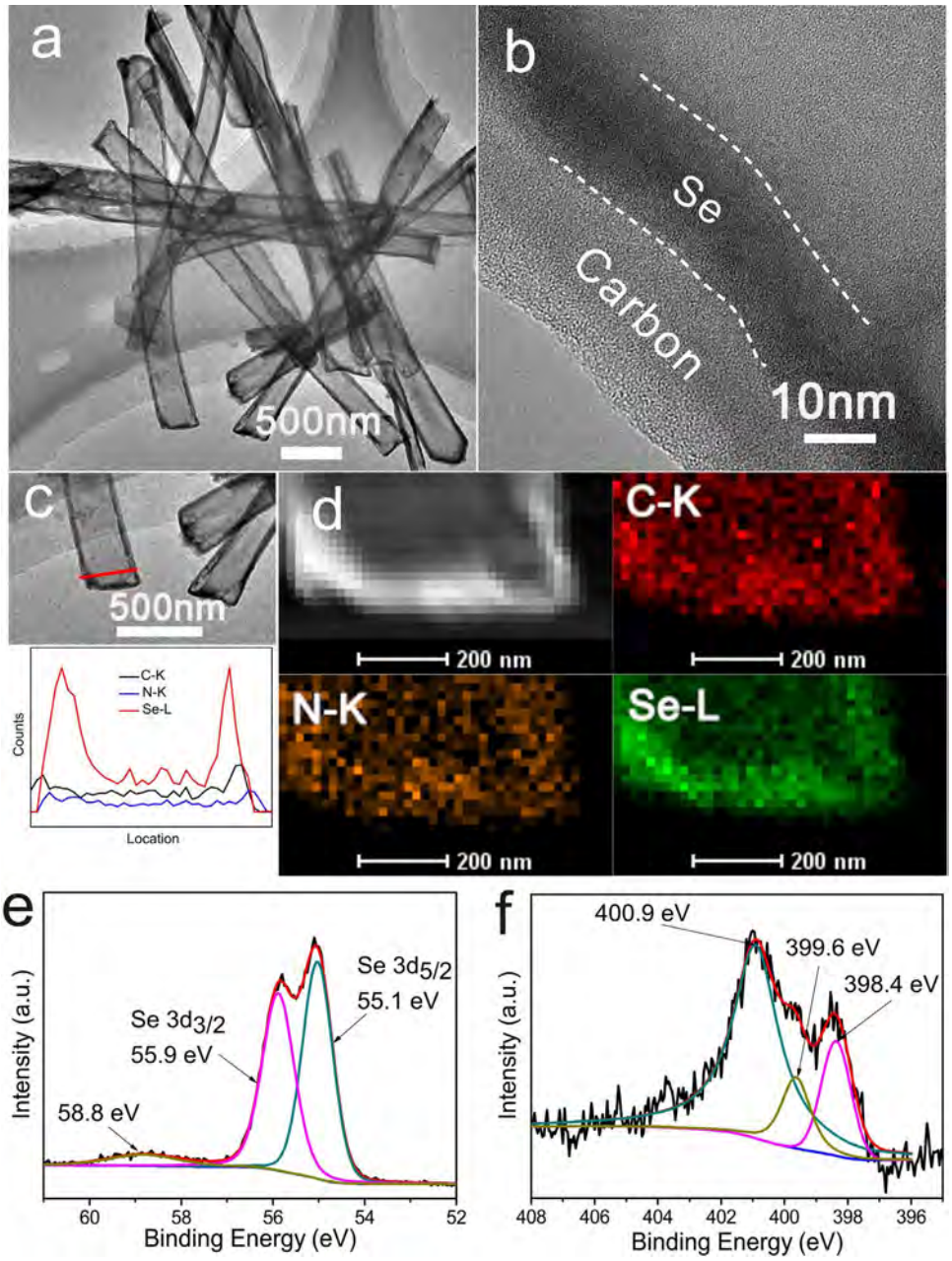


**Fig. 2.** (a) TEM image, (b) HR-TEM image, (c) EDS line scan, and (d) EDS elemental map of the double-shell Se@$CN_x$ nanobelts. (e) Fine XPS of Se 3d. (f) Fine XPS of N 1s.

hollow double-shelled Se@$CN_x$ nanobelts were measured by nitrogen adsorption/desorption experiments. The microporous characteristics can be observed from the $CN_x$ shell based on the nitrogen adsorption/desorption curve (Fig. S6, Supporting information). The measured BET surface of hollow double-shell Se@$CN_x$ nanobelts is 53.5 $m^2 g^{-1}$ and the pore diameter is mostly below 2 nm.

Boasting a large aspect ratio, the hollow double-shell Se@$CN_x$ nanobelts can readily form a self-supporting and flexible electrode film without needing a foreign binder or conducting additives. The paper-like freestanding Se@$CN_x$ cathode prepared by vacuum filtration shows robust mechanical flexibility (Fig. 3a). The cross-sectional SEM image shows that the self-supporting Se@$CN_x$ film has a thickness of about 30 μm (Fig. 3b). The enlarged cross-sectional SEM image shows that the film consists of intertwined and interpenetrated nanobelts forming a 3D interconnected NWs framework (Fig. S7, Supporting information). TG analysis (Fig. 4c) demonstrates that the Se content in the Se@$CN_x$ is about 62.5 wt%, which is much larger than that in most other Se/C electrodes (See Table 1). In addition, the Se content could be increased to 74 wt% by controlling the thickness of $CN_x$ shell as Fig. S8 (Supporting information) revealed.

To reveal the promising Li storage properties, the coin-like Li-Se batteries are assembled with the freestanding Se@$CN_x$ film as the cathode and Li as the anode. The electrolyte is 1 M $LiPF_6$ in ethylene (EC)/diethyl carbonate (DEC) (1:1 v/v). Fig. 4a shows typical cyclic voltammogram (CV) curves of the Se@$CN_x$ cathode for the first five cycles in the voltage range between 0.8 and 3.0 V at a scanning rate of 0.1 mV $s^{-1}$. In the cathodic curve, only one reduction peak at 1.70 V is observed, indicating that Se is converted directly into $Li_2Se$ without forming polyselenide intermediates in the carbonate electrolyte. This is in agreement with Guo's results using the same carbonate electrolyte based on the ring-structured $Se_8$ cathodes [23]. The cathodic peak shifts from 1.70 to 1.73 V after the 1st cycle due to electrochemical activation process [35] and the good overlap of the CV profiles after the 1st cycle indicates a stable and reversible electrochemical behavior during cycling. The charging and discharging voltage profiles of the double-shell Se@$CN_x$ nanobelts are depicted in Fig. 4b. The first 3

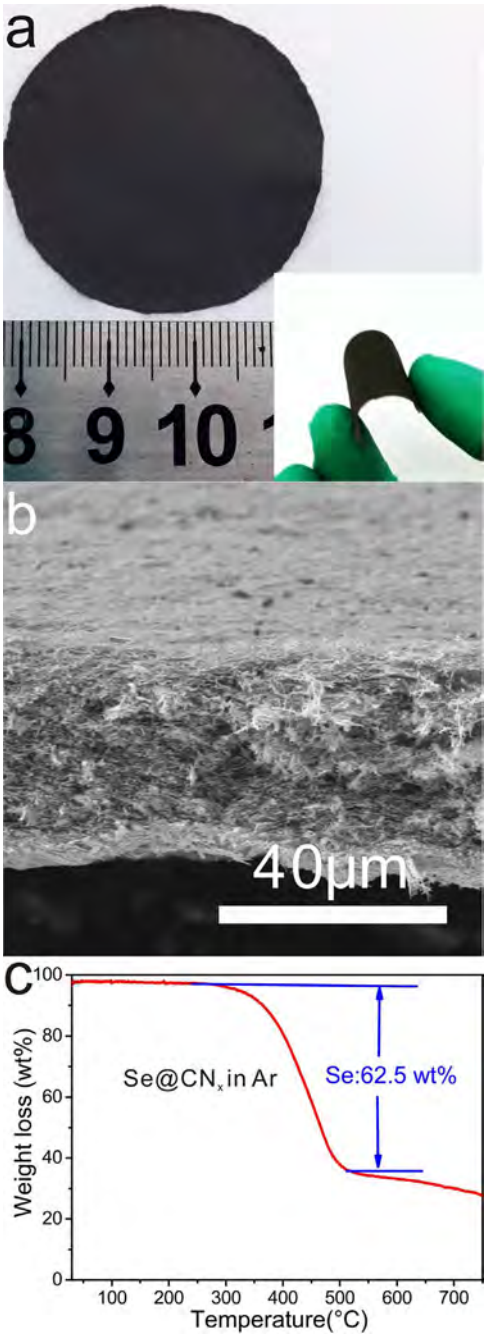


**Fig. 3.** (a) Optical image and (b) Side-view SEM images of the freestanding Se@$CN_x$ film. (c) TGA curve of hollow double-shell Se@$CN_x$ nanobelts.

cycles are measured at a density of 135 mA $g^{-1}$ and the following cycles are measured at 675 mA $g^{-1}$. The stable voltage plateau in the discharging curve corresponds to reduction of Se to $Li_2Se$ and the voltage plateau in the charging curve stems from oxidation of $Li_2Se$ to Se. The capacities in the first lithiation and delithiation processes are measured to be 904.8 mAh $g^{-1}$ (2.71 mAh $cm^{-2}$) and 730.3 mAh $g^{-1}$ (2.19 mAh $cm^{-2}$), respectively, indicating 80% Coulombic efficiency (CE). The initial irreversible capacity mainly comes from the outer $CN_x$ shell and activation of the Se@$CN_x$ electrode [36]. At a larger current density of 675 mA $g^{-1}$, the charging and discharging curves of the 10th and 100th cycles overlap suggesting excellent cycle stability. After 100 cycles, the double-shell Se@$CN_x$ nanobelts have a high capacity of 608.8 mAh $g^{-1}$ (1.83 mAh $cm^{-2}$) at a density of 675 mA $g^{-1}$ (1 C), corresponding to 90% Se utilization in comparison with the theoretical specific capacity of Se, which is higher than those reported from other Se-based cathode materials [37]. The long-term cycling stability of the Se@$CN_x$ cathode is evaluated and shown in Fig. 4c. The first 4 cycles are monitored at a current density of 80 mA $g^{-1}$ as an activation process and the following cycles are measured at 800 mA $g^{-1}$. With a large Se content of 62.5 wt% and areal mass loading of 3 mg $cm^{-2}$, the Se@$CN_x$ cathode deliver a reversible capacity of 597.4 mAh $g^{-1}$ after 6 cycles at 800 mA $g^{-1}$. After 400 cycles, a high capacity of 453.2 mAh $g^{-1}$ is obtained, implying 0.06% capacity decay per cycle from the 6th to 400th cycle. We also measure the electrochemical properties of $CN_x$ shells without Se, which are acquired by soaking the hollow double-shell Se@$CN_x$ nanobelts film in liquid $CS_2$ for one night to remove Se, followed by rinsing and vacuum drying. The charging and discharging voltage profiles and cycle stability of pure $CN_x$ nanobelts are depicted in Fig. S9 (Supporting information). The $CN_x$ delivers a capacity of 45.8 mAh $g^{-1}$ after 63 cycles at 500 mA $g^{-1}$. The content of $CN_x$ is 37.5 wt%, thus, the capacity contribution of the N-doped carbon is about 17.2 mAh $g^{-1}$, which is little and ignorable. Thus the capacity of the freestanding Se@$CN_x$ cathode is mainly from the Se active material. Fig. 4d shows the rate capability of the freestanding Se@$CN_x$ cathode. The specific capacities are measured to be 679, 656, 612, 539, and 474 mAh $g^{-1}$ at current densities of 80, 160, 320, 800, and 1600 mA $g^{-1}$, respectively. When the current density is increased from 80 to 1600 mA $g^{-1}$, 70% reversible capacity is retained. Moreover, when the current density is returned to 160 and 80 mA $g^{-1}$ after 30 cycles, the specific capacities recover to 656 and 683 mAh $g^{-1}$, respectively, implying that charging/discharging of freestanding Se@$CN_x$ cathode film is highly reversible even at large current densities.

To further verify the structural advantage of the hollow Se@$CN_x$ nanobelts, the Li-Se cell is disassembled after 400 cycles and Fig. 5a depicts the TEM image of the Se@$CN_x$ nanobelts after 400 cycles. The morphology of nanobelts is preserved after 400 cycles indicating excellent structural stability. The EDS elemental maps (Fig. 5b) and line scan (Fig. S10, Supporting information) acquired from the Se@$CN_x$ nanobelts reveal that Se, C, and N are uniformly distributed throughout the nanobelts after 400 cycles, further confirming excellent structural stability during cycling. Electrochemical impedance spectroscopy (EIS) performed on the Se@$CN_x$ cathode after the 1st and 400th cycles are shown in Fig. 5c and the equivalent circuit is shown in the inset of Fig. 5c. $R_s$ is the electrolyte resistance and a constant phase element (CPE1) in parallel with an ohmic resistance ($R_{ct}$) representing impedance of the charge transfer at the electrode/electrolyte interface [43,44]. The $R_{ct}$ decreases at the 400th cycle in comparison with the 1st cycle, implying a lower charge transfer resistance due to the electrolyte penetrating and activation. Hence the Se@$CN_x$ cathode exhibits a lower overpotential after activation as shown in Fig. 4a and b. The large specific capacity, good rate capability, and cycle stability can be attributed to the well-defined morphology of the hollow double-shell Se@$CN_x$ nanobelts. In the double-shell Se@$CN_x$ nanobelts, the void volume inside the $CN_x$ shell allows expansion of Se during the charging-discharging process and the $CN_x$ shell improves the electrical conductivity of the Se cathodes while providing some degree of physical entrapment for the polyselenide. Moreover, the self-supporting 3D interconnected conductive network comprising the conductive Se@$CN_x$ nanobelts without any binder improves the Se content in the cathode and facilitates electron and ion transfer during charging/discharging. Table 1 compare the electrochemical properties of the previously-reported Se/C composite with our hollow double-shell Se@C nanobelts, the Se-based cathode reported in this work exhibit larger Se mass loading, excellent cycle stability, higher capacity and rate performance.

## 4. Conclusions

In summary, hollow double-shell Se@$CN_x$ nanobelts are designed and fabricated as a freestanding and binder-free cathode for Li-Se battery, in which Se is fully confined and adheres to the inner surface of the hollow-core $CN_x$ nanobelts. The hollow double-shell Se@$CN_x$

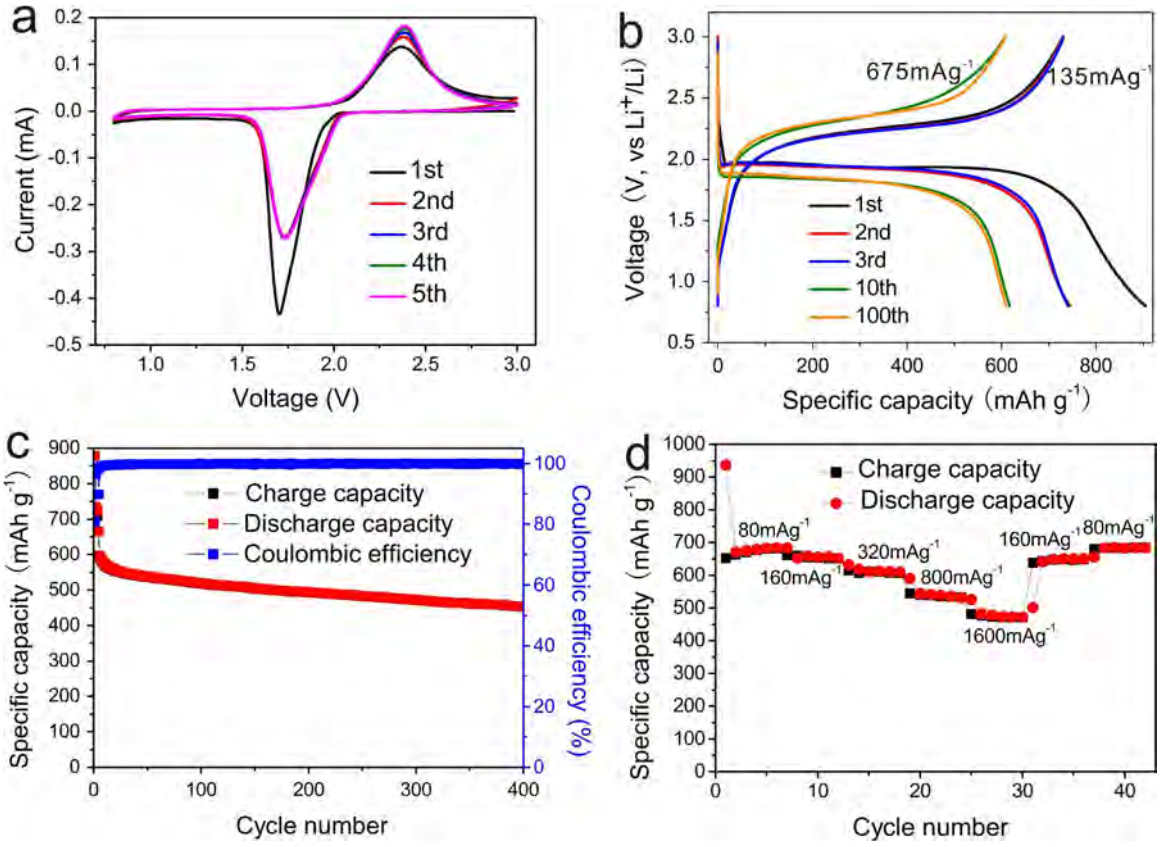


**Fig. 4.** Electrochemical performances of the freestanding hollow double-shell Se@$CN_x$ cathode film in the voltage range of 0.8–3.0 V: (a) CV curves at 0.1 mV $s^{-1}$ scanning rate. (b) Discharging-charging voltage profiles (the first 3 cycles were measured at a current density of 135 mA $g^{-1}$ and the following cycles at a current density of 675 mA $g^{-1}$). (c) Prolonged cycling performance and coulombic efficiency (the first 4 cycles were monitored at a current density of 80 mA $g^{-1}$ as an activation process and the following cycles at 800 mA $g^{-1}$). (d) Rate capability. The specific capacity is calculated based on the mass loading of Se in the cathode.

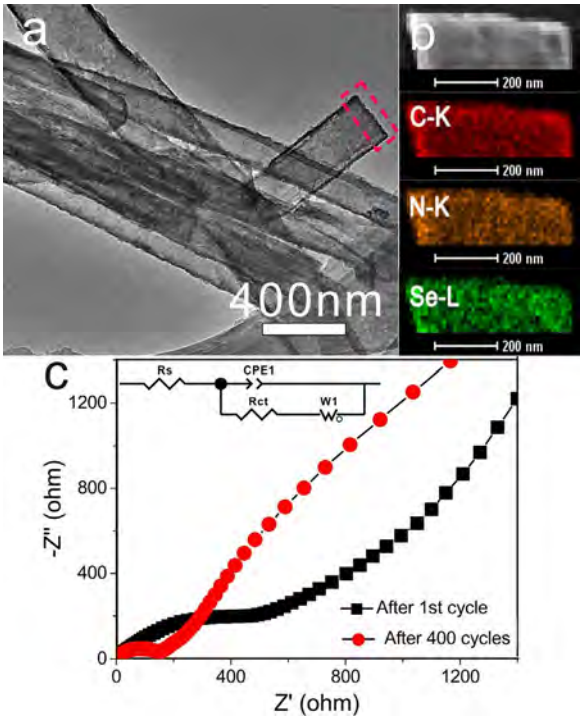


**Fig. 5.** (a) TEM image of the freestanding Se@$CN_x$ film cathode after 400 cycles. (b) EDS elemental maps of the Se@$CN_x$ composite after cycling. (c) Nyquist plots of the Se@$CN_x$ cathode after the 1st and 400th cycles. The inset is the equivalent circuit.

nanobelt provides a well-defined void volume to accommodate the volume expansion of Se upon lithiation and the $CN_x$ shell improves the electrical conductivity of the Se cathodes while providing some degree of physical entrapment for the Se and polyselenide. Boasting a large aspect ratio, a self-supporting, flexible, and binder-free electrode film comprising of intertwining and interpenetrating hollow double-shell Se@$CN_x$ nanobelts could be easily fabricated by simple vacuum filtration without needing any binder and conductive additives. The paper-like Se@$CN_x$ cathode has a large Se mass loading of 62.5 wt%. With a large areal loading of 3 mg $cm^{-2}$, the freestanding cathode of Se@$CN_x$ nanobelts deliver a high capacity of 608.8 mAh $g^{-1}$ in a carbonate-based electrolyte at the density of 675 mA $g^{-1}$ after 100 cycles and the cycle stability is maintained for over 400 cycles with only 0.06% capacity decay per cycle. The self-supporting freestanding Se@$CN_x$ cathode comprising intertwining and interpenetrating Se@$CN_x$ nanobelts has a high conductivity and facilitates electrons and ions transfer, leading to high rate capability. When the current density is increased 20 times from 80 to 1600 mA $g^{-1}$, 70% reversible capacity is observed. The excellent electrochemical performance of Se@$CN_x$ nanobelts arise from the well-defined hollow double-shell morphology, high conductivity and high Se content in the self-supporting flexible cathode, which bodes well for their application to stretchable/bendable energy storage devices.

## Acknowledgements

This work was financially supported by the National Natural Science Foundation of China (No. 52572100), the Natural Science Foundation of Hubei Province (2015CFA116), Fundamental Research Funds for the Central Universities (HUST: 2015QN071), Outstanding Young and Middle-aged Scientific Innovation Team of Colleges and

Universities of Hubei Province (T201402), and City University of Hong Kong Applied Research Grant (ARG) no. 9667122. We also acknowledge the Nanodevices and Characterization Center of WNLO-HUST and Analytical and Testing Center of HUST.

## Appendix A. Supplementary material

Supplementary data associated with this article can be found in the online version at http://dx.doi.org/10.1016/j.nanoen.2016.12.010.

## References

[1] B. Goodenough, K.S. Park, J. Am. Chem. Soc. 135 (2013) 1167–1176.
[2] J. Wang, H. Tang, L. Zhang, H. Ren, R. Yu, Q. Jin, J. Qi, D. Mao, M. Yang, Y. Wang, P. Liu, Y. Zhang, Y. Wen, L. Gu, G. Ma, Z. Su, Z. Tang, H. Zhang, D. Wang, Nat. Energy 1 (2016) 16050.
[3] H. Ren, J. Sun, R.B. Yu, M. Yang, L. Gu, P. Liu, H. Zhao, D. Kisailus, D. Wang, Chem. Sci. 7 (2016) 793–798.
[4] J. Qi, X.Y. Lai, J.Y. Wang, H.J. Tang, H. Ren, Y. Yang, Q. Jin, L.J. Zhang, R.B. Yu, G.H. Ma, Z.G. Su, H.J. Zhao, D. Wang, Chem. Soc. Rev. 44 (2015) 6749–6773.
[5] H. Ren, R. Yu, J. Wang, Q. Jin, M. Yang, D. Mao, D. Kisailus, H. Zhao, D. Wang, Nano Lett. 14 (2014) 6679–6684.
[6] S. Xu, C.M. Hessel, H. Ren, R.B. Yu, Q. Jin, M. Yang, H. Zhao, D. Wang, Energy Environ. Sci. 7 (2014) 632–637.
[7] J. Wang, N. Yang, H. Tang, Z. Dong, Q. Jin, M. Yang, D. Kisailus, H. Zhao, Z. Tang, D. Wang, Angew. Chem. Int. Ed. 52 (2013) 6417–6420.
[8] H.J. Tang, C.M. Hessel, J.Y. Wang, N.L. Yang, R.B. Yu, H.J. Zhao, D. Wang, Chem. Soc. Rev. 43 (2014) 4281–4299.
[9] C. Chen, Y. Wen, X. Hu, X. Ji, M. Yan, L. Mai, P. Hu, B. Shan, Y. Huang, Nat. Commun. 6 (2015) 6929.
[10] M. Armand, J.M. Tarascon, Nature 451 (2008) 652–657.
[11] Y.K. Sun, S.T. Myung, B.C. Park, J. Prakash, I. Belharouak, K. Amine, Nat. Mater. 8 (2009) 320–324.
[12] Y.M. Chiang, Science 330 (2010) 1485–1486.
[13] X.L. Ji, L.F. Nazar, J. Mater. Chem. 20 (2010) 9821–9826.
[14] P.G. Bruce, S.A. Freunberger, L.J. Hardwick, J.M. Tarascon, Nat. Mater. 11 (2012) 19–29.
[15] Y.X. Yin, S. Xin, Y.G. Guo, L.J. Wan, Angew. Chem. Int. Ed. 52 (2013) 13186–13200.
[16] S.Y. Chung, J.T. Bloking, Y.M. Chiang, Nat. Mater. 1 (2002) 123–128.
[17] S.E. Cheon, K.S. Ko, J.H. Cho, S.W. Kim, E.Y. Chin, H.T. Kim, J. Electrochem. Soc. 150 (2003) A796–A799.
[18] X. Ji, K.T. Lee, L.F. Nazar, Nat. Mater. 8 (2009) 500–506.
[19] C.P. Yang, Y.X. Yin, Y.G. Guo, J. Phys. Chem. Lett. 6 (2015) 256–266.
[20] C. Luo, Y. Xu, Y. Zhu, Y. Liu, S. Zheng, Y. Liu, A. Langrock, C. Wang, ACS Nano 7 (2013) 8003–8010.
[21] J.T. Lee, H. Kim, M. Oschatz, D.C. Lee, F. Wu, H.T. Lin, B. Zdyrko, W.I. Cho, S. Kaskel, G. Yushin, Adv. Energy Mater. 5 (2014) 1400981.
[22] J.J. Zhang, L. Fan, Y. Zhu, Y. Xu, J. Liang, D. Wei, Y.T. Qian, Nanoscale 6 (2014) 12952–12957.
[23] C.P. Yang, S. Xin, Y.X. Yin, H. Ye, J. Zhang, Y.G. Guo, Angew. Chem. Int. Ed. 52 (2013) 8363–8367.
[24] Z. Li, L. Yuan, Z. Yi, Y. Liu, Y. Huang, Nano Energy 9 (2014) 229–236.
[25] B.W. Yao, S.H. Yu, X. Huang, J. Jiang, L.Q. Zhao, L. Pan, J. Li, Adv. Mater. 17 (2005) 2799–2802.
[26] H. Ye, Y.X. Yin, S.F. Zhang, Y.G. Guo, J. Mater. Chem. A 2 (2014) 13293–13298.
[27] V.V. Poborchii, A.V. Kolobov, K. Tanaka, Appl. Phys. Lett. 72 (1998) 1167–1169.
[28] I.L. Li, J.P. Zhai, P. Launois, S.C. Ruan, Z.K. Tang, J. Am. Chem. Soc. 127 (2005) 16111–16119.
[29] I.L. Li, S. Ruan, Z. Li, J. Zhai, Z. Tang, Appl. Phys. Lett. 87 (2005) 071902.
[30] S. Maldonado, S. Morin, K.J. Stevenson, Carbon 44 (2006) 1429–1437.
[31] F.B. Su, C.K. Poh, J.S. Chen, G.W. Xu, D. Wang, Q. Li, J.Y. Lin, X.W. Lou, Energy Environ. Sci. 4 (2011) 717–724.
[32] Y. Cui, A. Abouimrane, J. Lu, T. Bolin, Y. Ren, W. Weng, C. Sun, V.A. Maroni, S.M. Heald, K. Amine, J. Am. Chem. Soc. 135 (2013) 8047–8056.
[33] Y. Liu, L. Si, Y. Du, X. Zhou, Z. Dai, J. Bao, J. Phys. Chem. C 119 (2015) 27316–27321.
[34] Z.H. Sheng, L. Shao, J.J. Chen, W.J. Bao, F.B. Wang, X.H. Xia, ACS Nano 5 (2011) 4350–4358.
[35] Y. Liu, L. Si, X. Zhou, X. Liu, Y. Yu, J. Bao, Z. Dai, J. Mater. Chem. A 2 (2014) 17735–17739.
[36] J. Zhang, Y. Xu, L. Fan, Y. Zhu, J. Liang, Y.T. Qian, Nano Energy 13 (2015) 592–600.
[37] J. Guo, Q. Wang, C. Qi, J. Jin, Y. Zhu, Z. Wen, Chem. Commun. 52 (2016) 5613–5616.
[38] K. Han, Z. Liu, H. Ye, F. Dai, J. Power Sources 263 (2014) 85–89.
[39] S. Jiang, Z. Zhang, Y. Lai, Y. Qu, X. Wang, J. Li, J. Power Sources 267 (2014) 394–404.
[40] L. Liu, Y. Wei, C. Zhang, C. Zhang, X. Li, J. Wang, L. Ling, W. Qiao, D. Long, Electrochim. Acta 153 (2015) 140–148.
[41] Y. Jiang, X. Ma, J. Feng, S. Xiong, J. Mater. Chem. A 3 (2015) 4539–4546.
[42] T. Liu, C. Dai, M. Jia, D. Liu, S. Bao, J. Jiang, M. Xu, C.M. Li, A.C.S. Appl, Mater. Interfaces 8 (2016) 16063–16070.
[43] C. Luo, Y. Zhu, Y. Wen, J. Wang, C. Wang, Adv. Funct. Mater. 24 (2014) 4082–4089.
[44] Z. Li, L. Yin, Nanoscale 7 (2015) 9597–9606.

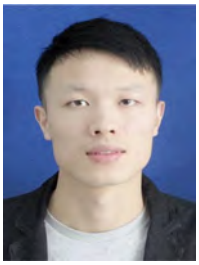

**Qifa Cai** received his B.S. degree from Hubei University of Technology in 2014. Currently, he is a graduate student in the Wuhan National Laboratory for Optoelectronics (WNLO) at Huazhong University of Science and Technology (HUST), under the supervision of Prof. Kaifu Huo. His research interests mainly focus on Li-S (Se) batteries.

**Yuanyuan Li** received her M.S. degree from Key Laboratory for Special Functional Materials of the Ministry of Education, Henan University, China in 2013. She is currently a Ph.D. candidate in the Wuhan National Laboratory for Optoelectronics (WNLO), Huazhong University of Science and Technology (HUST) under supervision of Prof. Kaifu Huo. Her present research interests mainly focus on Li-S batteries.

**Lei Wang** earned his B.S. degree in physics from Huazhong University of Science and Technology (HUST) in 2012. He is currently a Ph.D. candidate in the Wuhan National Laboratory for Optoelectronics (WNLO) at Huazhong University of Science and Technology (HUST), under the supervision of Prof. Kaifu Huo. His present research interest is the synthesis of synthesis and characterization of nanostructured electrode architectures and materials for electrochemical energy conversion and storage.

**Qingwei Li** earned his B.E. degree (2007) from Chang'an University and received M.S. degree (2011) from Henan University. Now, he is a Ph.D. candidate in the Wuhan National Laboratory for Optoelectronics (WNLO) at Huazhong University of Science and Technology (HUST), under the supervision of Prof. Kaifu Huo. His research interests focus on the controllable synthesis of nanomaterials for energy storage and conversion.

**Juan Xu** earned her B.S. degree in physics in Xinxiang University in 2012. Now, she is a Ph.D. candidate under the supervision of Prof. Kaifu Huo in the Wuhan National Laboratory for Optoelectronics (WNLO) at Huazhong University of Science and Technology (HUST). Her research interests mainly focus on synthesis of metal oxides materials for lithium ion batteries and lithium ion hybrid capacitors.

**Biao Gao** received his M.S. and Ph.D. in Material Science from Wuhan University of Science and Technology in 2012 and 2016. He is currently a lecture in the state key laboratory of refractories and metallurgy at Wuhan University of Science and Technology. His main research activities encompass nanostructured functional ceramic and nanomaterials for electrochemical energy storage.

**Xuming Zhang** received his Ph.D. in materials science and engineering from City University of Hong Kong in 2015 and worked for one year as a senior research associate in the Plasma Laboratory at City University of Hong Kong under the supervision of Prof. Paul K. Chu. He is now working as professor in Wuhan University of Science and Technology. His research interests on the synthesis of nanomaterials for application in electrochemical sensors, electrochemical catalysis, and electrochemical energy storage devices.

**Kaifu Huo** received his B.S. in Applied Chemistry from China University of Petroleum in 1997 and a Ph.D. in Physical Chemistry from Nanjing University (China) in 2004. He is currently a full Professor in the National Laboratory for Optoelectronics (WNLO) at Huazhong University of Science and Technology. He is an associate editor of Nanoscience and Nanotechnology Letters. He has authored/co-authored more than 100 papers in peer-reviewed international journals. His main research activities encompass bioactive nanomaterials and nanostructured electrode materials for electrochemical biosensors and energy storage devices.

**Paul K. Chu** received his Ph.D. in Chemistry from Cornell University. He is Chair Professor of Materials Engineering in the Department of Physics and Materials Science at City University of Hong Kong. He is Fellow of the American Physical Society (APS), American Vacuum Society (AVS), Institute of Electrical and Electronics Engineers (IEEE), Materials Research Society (MRS), and Hong Kong Institution of Engineers (HKIE). He is also Fellow of the Hong Kong Academy of Engineering Sciences (HKAES). His research interests are quite diverse encompassing plasma surface engineering, materials science and engineering, surface science, and functional materials.

# Supporting Information

## Freestanding Hollow Double-Shell Se@$CN_x$ Nanobelts as Large-Capacity and High-Rate Cathodes for Li-Se Batteries

Qifa Cai, [a] Yuanyuan Li, [a] Lei wang, [a] Qingwei Li, [a,c] Juan Xu, [a] Biao Gao, [b] Xuming Zhang, [b,c] Kaifu Huo [a,*] and Paul K Chu [c]

[a] Wuhan National Laboratory for Optoelectronics (WNLO) and School of Optical and Electronic Information, Huazhong University of Science and Technology, Wuhan 430074, China.

[b] The State Key Laboratory of Refractories and Metallurgy, Wuhan University of Science and Technology, Wuhan 430081, China.

[c] Department of Physics and Materials Science, City University of Hong Kong, Tat Chee Avenue, Kowloon, Hong Kong, China.

*Corresponding Authors: E-mail: kfhuo@hust.edu.cn

**Six pages**

**Figure S1-Figure S10**

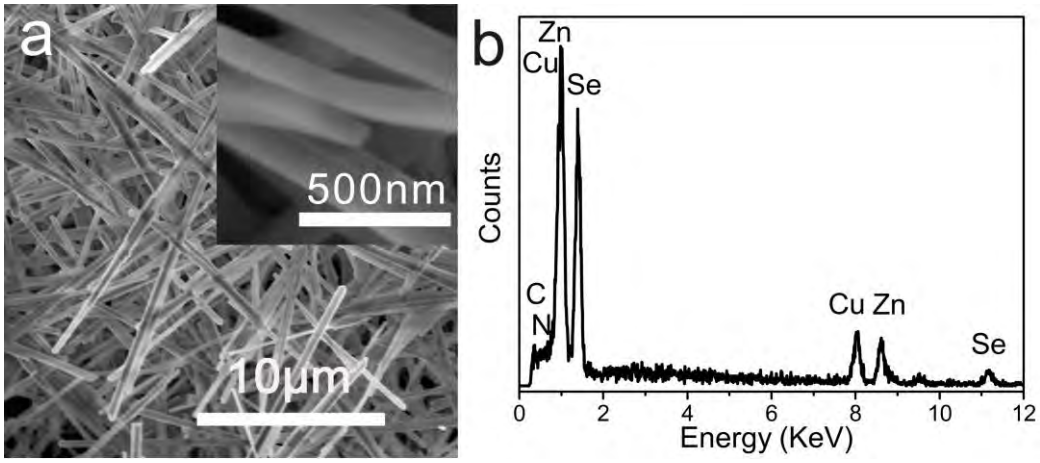


**Figure S1.** a) SEM image, b) EDS of $ZnSe[DETA]_{0.5}$.

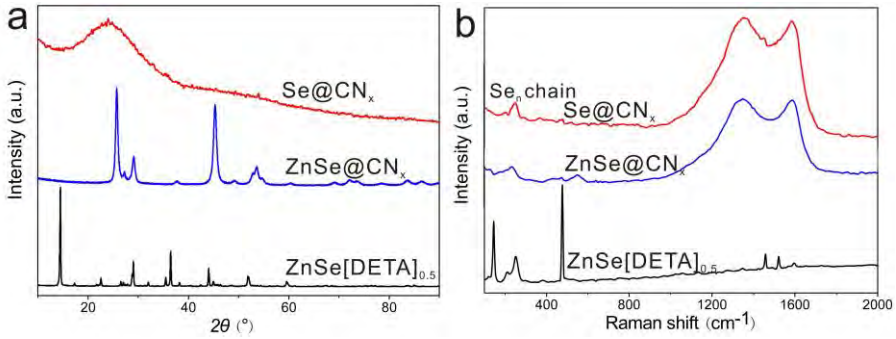


**Figure S2.** a) X-ray diffraction patterns and b) Raman spectra of $ZnSe[DETA]_{0.5}$, core-shell $ZnSe@CN_x$ and hollow double-shell $Se@CN_x$.

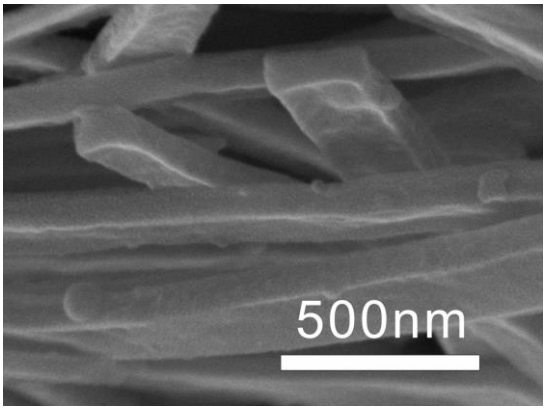


**Figure S3.** Cross-section SEM image of double-shell Se@$CN_x$ nanobelts

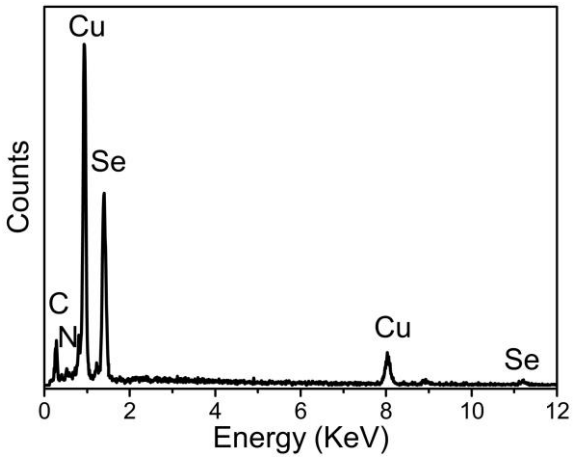


**Figure S4.** EDS spectra of Se@$CN_x$ nanobelts.

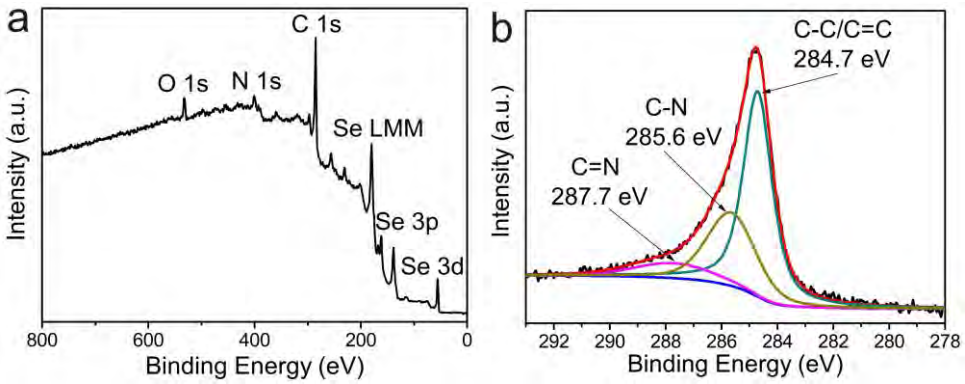


**Figure S5.** a) XPS survey spectra of double-shell Se@$CN_x$ nanobelts; b) Fine C 1s spectrum, the C1s can be divided into three peaks which are C-C/C=C(284.7 eV), C-N(285.6 eV), C=N(287.7 eV).[1]

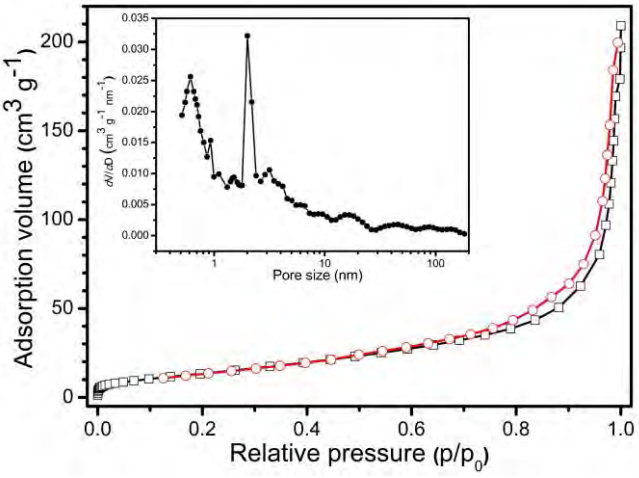


**Figure S6.** Pore size distribution of $Se@CN_x$

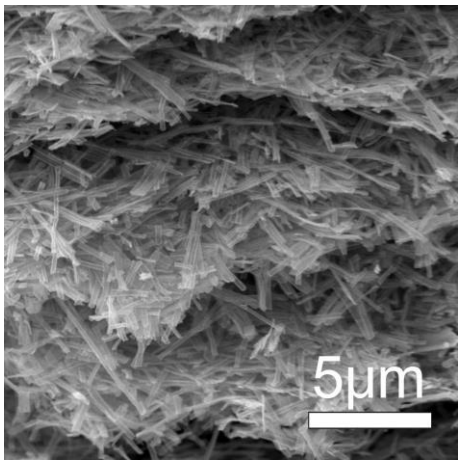


**Figure S7.** Side-view SEM images of the $Se@CN_x$ film.

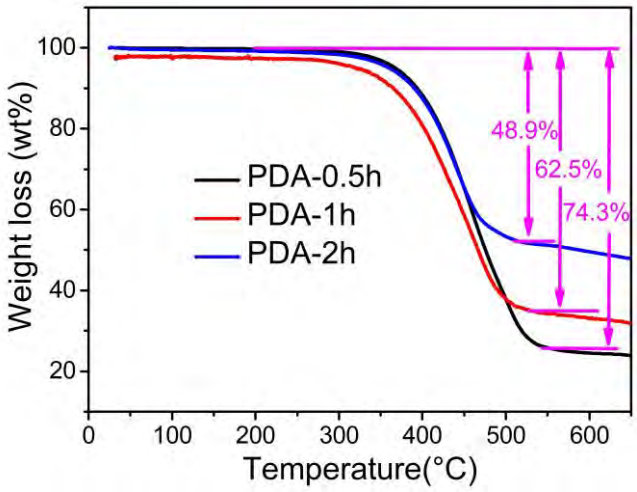


**Figure S8.** TGA curves of hollow double-shell Se@$CN_x$ nanobelts with the different time of dopamine self-polymerization (0.5, 1 and 2h), respectively.

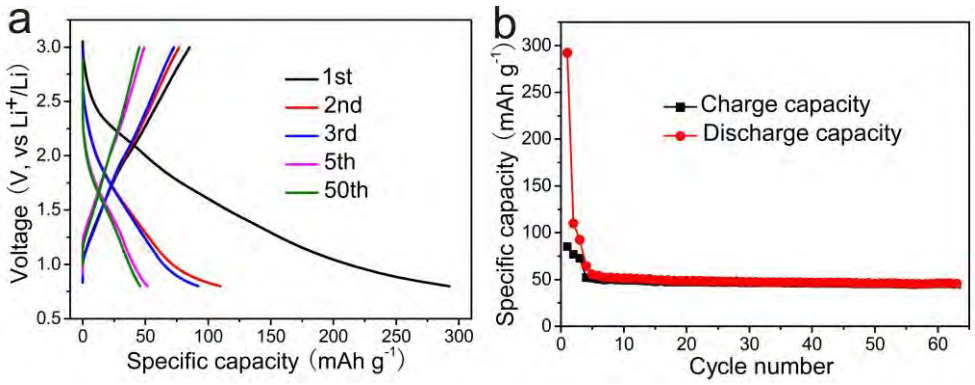


**Figure S9.** Electrochemical performances of the $CN_x$ cathode film in the voltage range of 0.8-3.0 V: a) Discharging-charging voltage profiles (the first three cycles was measured at a current density of 50 mA $g^{-1}$ and the following cycles at a current density of 500 mA $g^{-1}$). b) Cycling performance.

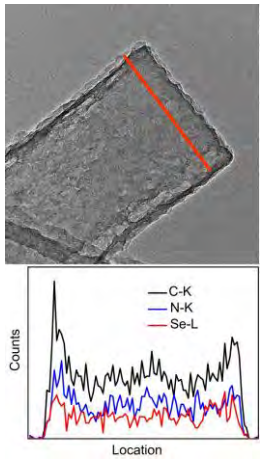


**Figure S10.** EDS Line scan of the Se@$CN_x$ composite after cycling.

## REFERENCES

[1] R. A. Zangmeister, T. A. Morris, M. J. Tarlov, Langmuir 29(2013) 8619-8628.